Usefulness of Fasting ^{18}F-FDG PET in Identification of Cardiac Sarcoidosis

Wataru Okumura, MD[1]; Tsutomu Iwasaki, MD[1]; Takuji Toyama, MD[1]; Tatsuya Iso, MD[1]; Masashi Arai, MD[1]; Noboru Oriuchi, MD[2]; Keigo Endo, MD[2]; Tomoyuki Yokoyama, MD[3]; Tadashi Suzuki, MD[4]; and Masahiko Kurabayashi, MD[1]

[1]Second Department of Internal Medicine, Gunma University School of Medicine, Maebashi, Japan; [2]Department of Diagnostic Radiology and Nuclear Medicine, Gunma University School of Medicine, Maebashi, Japan; [3]Department of Laboratory Sciences, Gunma University School of Health Science, Maebashi, Japan; and [4]Fujioka General Hospital, Fujioka, Japan

Cardiac PET using ^{18}F-FDG under fasting conditions (fasting ^{18}F-FDG PET) is a promising technique for identification of cardiac sarcoidosis and assessment of disease activity. The aim of this study was to investigate the usefulness of fasting ^{18}F-FDG PET in detecting inflammatory lesions of cardiac sarcoidosis from a pathophysiologic standpoint. **Methods:** Twenty-two patients with systemic sarcoidosis were classified into 2 groups of 11 each according to the presence or absence of sarcoid heart disease. Cardiac sarcoidosis was diagnosed according to the Japanese Ministry of Health and Welfare guidelines for diagnosing cardiac sarcoidosis with the exception of scintigraphic criteria. Nuclear cardiac imaging with fasting ^{18}F-FDG PET, ^{99m}Tc-methoxyisobutylisonitrile (^{99m}Tc-MIBI) SPECT, and ^{67}Ga scintigraphy were performed in all patients. PET and SPECT images were divided into 13 myocardial segments and the standardized uptake value (SUV) of ^{18}F-FDG was calculated and defect scores (DS) for ^{99m}Tc-MIBI uptake were assessed for each segment. The total SUV (T-SUV) and total DS (TDS) were calculated as the sum of measurements for all 13 segments, and the diagnostic accuracy of fasting ^{18}F-FDG PET was compared with that of the other nuclear imaging modalities. In addition, pathophysiologic relationships between inflammatory activity and myocardial damage were examined by segmental comparative study using the SUV and DS. **Results:** In patients with cardiac sarcoidosis, fasting ^{18}F-FDG PET revealed a higher frequency of abnormal myocardial segments than ^{99m}Tc-MIBI SPECT (mean number of abnormal segments per patient: 6.6 ± 3.0 vs. 3.0 ± 3.2 [mean $\pm$ SD], $P < 0.05$). The sensitivity of fasting ^{18}F-FDG PET in detecting cardiac sarcoidosis was 100%, significantly higher than that of ^{99m}Tc-MIBI SPECT (63.6%) or ^{67}Ga scintigraphy (36.3%). The accuracy of fasting ^{18}F-FDG PET was significantly higher than ^{67}Ga scintigraphy. The T-SUV demonstrated a good linear correlation with serum angiotensin-converting enzyme levels ($r = 0.83$, $P < 0.01$), and the TDS showed a significant negative correlation with the left ventricular ejection fraction ($r = -0.82$, $P < 0.01$). In abnormal myocardial segments on the nuclear scan, the SUV showed a significant negative correlation with the DS ($r = -0.63$, $P < 0.0001$). **Conclusion:** This study suggests that fasting ^{18}F-FDG PET can detect the early stage of cardiac sarcoidosis, in which fewer perfusion abnormalities and high inflammatory activity are noted, before advanced myocardial impairment.

Key Words: PET; ^{18}F-FDG; fasting; cardiac sarcoidosis

J Nucl Med 2004; 45:1989–1998

S arcoidosis is a systemic disorder of unknown cause that is characterized by its pathologic hallmark, the noncaseating granuloma. Although the disease is generally associated with a low mortality rate, cardiac involvement may carry a poor prognosis. Myocardial involvement is present in 20%–76% of patients with sarcoidosis (*1,2*) and is responsible for as many as 77% of deaths from the disease (*3*). Although endomyocardial biopsy is required for definitive diagnosis of cardiac sarcoidosis, it is invasive and may lack sensitivity because myocardial involvement is not homogeneous. Scintigraphy using ^{67}Ga, ^{201}Tl, and ^{99m}Tc-methoxyisobutylisonitrile (^{99m}Tc-MIBI) are also used to detect cardiac involvement in patients with sarcoidosis (*4–6*). An abnormal perfusion area on ^{201}Tl or ^{99m}Tc-MIBI SPECT is considered as impaired myocardium, although myocardial perfusion defects are not specific to sarcoidosis and can occur with ischemic heart disease or other cardiomyopathies (*4,5*). Furthermore, although accumulation of ^{67}Ga is considered an indicator of inflammatory change, ^{67}Ga scintigraphy is an insensitive method for detection of cardiac involvement in sarcoidosis (*7*). Recent studies have revealed that ^{18}F-FDG PET under fasting conditions (fasting ^{18}F-FDG PET) is a useful method for identification of cardiac sarcoidosis and for assessment of disease activity (*7,8*). However, to our knowledge, no investigations have been published with regard to the usefulness of fasting ^{18}F-FDG PET in detecting cardiac sarcoidosis that take into account pathophysiologic considerations. The present study was designed to evaluate the usefulness of fasting ^{18}F-FDG PET in detecting inflammatory lesions of cardiac sarcoidosis from a pathophysiologic standpoint, based on correlative analysis between the uptake pattern in combined nuclear imaging stud-

TABLE 1
Characteristics of 22 Patients

Patient no.	Age (y)	Sex	ECG findings	LVEF (%)	Histologic diagnosis of extracardiac sarcoidosis	Blood glucose (mg/dL)	Serum ACE (IU/L 37°C)
Group A							
1	69	M	Complete AVB	41	Myocardium	103	7.4
2	69	F	Second AVB	45	Myocardium	85	8.8
3	65	F	ST–T change, VT	33	Myocardium	82	12.3
4	73	F	ST–T change, second AVB	47	Intraabdominal LN	91	14.4
5	52	F	CRBBB, ST–T change, VT	71	TBLB	76	12.5
6	46	F	CRBBB + LAH, second AVB	40	TBLB	74	30.1
7	55	F	CRBBB + LAH, first AVB, VT	42	Scalene node	104	11.1
8	78	F	ST–T change, second AVB	67	Scalene node	92	13.4
9	73	F	Second AVB, PSVT	57	Skin	94	22.4
10	62	F	CRBBB + LAH, VT	47	Skin	72	30.0
11	62	F	Second AVB	68	Skin	81	18.3
Group B							
12	62	F	Normal	71	TBLB	95	3.5
13	54	F	CRBBB	80	TBLB	85	19.7
14	44	M	Normal	78	TBLB	77	30.2
15	37	F	Normal	60	TBLB	84	39.3
16	56	F	Normal	76	TBLB	102	12.5
17	74	F	CRBBB	82	Scalene node	79	20.7
18	67	M	Normal	67	Scalene node	101	12.1
19	66	F	Normal	67	Skin	92	27.8
20	71	F	Normal	68	Skin	74	11.2
21	64	F	Normal	75	Skin	82	26.0
22	68	F	ST–T change	73	Skin	104	18.0

ECG = electrocardiography; LVEF = left ventricular ejection fraction; ACE = angiotensin-converting enzyme; AVB = atrioventricular block; VT = ventricular tachycardia; LN = lymph node; CRBBB = complete right bundle branch block; TBLB = transbronchial lung biopsy; LAH = left anterior hemiblock; PSVT = paroxymal supraventricular tachycardia.

ies and the clinical and histologic findings in patients with cardiac sarcoidosis.

MATERIALS AND METHODS

Patients and Healthy Subjects

Patients. Twenty-two patients (3 men, 19 women; mean age, 62.1 y; range, 37–78 y) with active sarcoidosis were prospectively recruited into this study. Diagnosis was confirmed histologically by the presence of noncaseating granulomas on intraabdominal lymph node biopsy (patient 4), transbronchial lung biopsy (patients 5, 6, and 12–16), scalene node biopsy (patients 7, 8, 17, and 18), skin biopsy (patients 9–11 and 19–22), or endomyocardial biopsy (patients 1–3). No patients showed evidence of diabetes mellitus. Patient details are given in Table 1. The 22 patients were classified into 2 groups according to the presence or absence of clinically well-documented sarcoid heart disease. Eleven patients had evidence of cardiac sarcoidosis (group A) and the other 11 patients did not (group B). Cardiac sarcoidosis was diagnosed according to the relevant Japanese Ministry of Health and Welfare guidelines for diagnosing cardiac sarcoidosis described in Table 2 (*9*), but criterion 2c was not used to avoid the bias from the analysis. The serum angiotensin-converting enzyme (ACE) level was measured in all patients treated without ACE inhibitors. Endomyocardial biopsy was performed in all patients in group A, and 2 or 3 specimens were obtained from the left ventricle. Diagnosis of

sarcoid heart disease, based on the presence of noncaseating granulomas on endomyocardial biopsy (histologic cardiac sarcoidosis), was made in 3 patients (patients 1–3) who showed atrioventricular block or intractable ventricular tachycardia. In the patients without histologic evidence on endomyocardial biopsy, sarcoid heart disease was diagnosed based on the presence of severe unexplained cardiac problems, including echocardiographically proven ventricular dysfunction, serious ventricular arrhythmia (≥grade 2, Lown's classification), or second- or third-degree atrioventricular block (patients 4–11: clinical cardiac sarcoidosis). Cardiac catheterization, including selective coronary angiography, was performed in patients with sarcoid heart disease and failed to reveal atherosclerotic stenoses.

Healthy Subjects. Seven healthy volunteers (mean age, 46.0 y; range, 37–65 y) were studied to obtain reference values for the standardized uptake value (SUV) of ^{18}F-FDG in the heart.

Written informed consent was obtained from all patients and volunteers, and the study protocol was approved by the institutional ethics committee and radiation protection authorities.

Imaging Protocol

Within a 2-wk period after entering the study, all patients underwent ^{18}F-FDG myocardial PET, ^{99m}Tc-MIBI myocardial SPECT, and ^{67}Ga scintigraphy.

^{18}F-FDG PET. Whole-body ^{18}F-FDG dedicated PET was performed with a SET 2400W (Shimadzu Corp.) with a 59.5-cm

TABLE 2
Guidelines for Diagnosis of Cardiac Sarcoidosis from Japanese Ministry of Health and Welfare

Criterion for diagnosis of cardiac sarcoidosis

1: Histologic diagnosis group
  Cardiac sarcoidosis is diagnosed when histologic analysis of operative or endomyocardial biopsy specimens demonstrates epithelioid granuloma without caseating granuloma.

2: Clinical diagnosis group
  In patients with histologic diagnosis of extracardiac sarcoidosis, cardiac sarcoidosis is diagnosed when item "a" and one or more of items "b–e" are present.

  a. Complete right bundle branch block, left-axis deviation, atrioventricular block, ventricular tachycardia, premature ventricular contraction (more than second grade of Lown's classification), or abnormal Q or ST–T change on electrocardiogram or ambulatory electrocardiogram

  b. Abnormal wall motion, regional wall thinning or thickening, or dilatation of left ventricle on echocardiogram

  c. Perfusion defect in ^{201}T1 myocardial scintigraphy or abnormal accumulation in ^{67}Ga-citrate or ^{99m}Tc-pyrophosphate myocardial scintigraphy

  d. Abnormal intracardiac pressure, low cardiac output, or abnormal wall motion or depressed ejection fraction of left ventricle

  e. Interstitial fibrosis or cellular infiltration over moderate grade in endomyocardial biopsy even if findings are nonspecific

---

transaxial field of view and 20-cm axial view that produced 63 image planes spaced 3.125 mm apart. All patients fasted for at least 12 h before the examination, and plasma glucose levels were measured before injection of the tracer. Simultaneous emission–transmission scans were obtained 1 h after injection of approximately 200 MBq (5.4 mCi) of ^{18}F-FDG. The performance characteristics of this scanner and processing methods have been described previously (10).

^{99m}Tc-MIBI SPECT and ^{67}Ga Scintigraphy. In all patients, ^{99m}Tc-MIBI SPECT for myocardial perfusion imaging and ^{67}Ga scintigraphy were performed. Myocardial SPECT data acquisition commenced 40–50 min after intravenous injection of the tracer (600 MBq of ^{99m}Tc-MIBI) during rest and after at least 12 h of fasting. To remove ^{99m}Tc-MIBI accumulated in the gallbladder, all patients drank milk between tracer injection and image acquisition.

With a triple-head SPECT γ-camera (Prism 3000; Marconi/Shimadzu) equipped with low-energy, general-purpose collimators, a total of 20 projection images were obtained over 360° in 6° increments, at 50 s per view. Myocardial SPECT data were processed by filtered backprojection (Butterworth filter, cutoff frequency at 0.2 cycle/pixel; order, 4).

^{67}Ga scintigraphic imaging was performed 72 h after intravenous injection of 74 MBq of ^{67}Ga citrate. Views were obtained with a large-field γ-scintillation camera (Prism 2000; Picker) with 3 photopeaks (93, 184, and 296 keV) equipped with a medium-energy, general-purpose collimator. Anterior and posterior views of the thorax were obtained.

Image Analysis

Functional images of the SUV were produced from attenuation-corrected images, with reference to the injected dose of ^{18}F-FDG, body weight, and cross-calibration factors between PET and the dose calibrator. SUV was defined as follows:

$$SUV = \frac{\text{Radioactivity concentration in ROI (Bq} \cdot \text{mm}^{-3})}{\text{Injection dose (Bq)/weight of patient (g)}}.$$

For the analysis of myocardial accumulation of ^{18}F-FDG, a polygonal region of interest (ROI) for each of the 13 myocardial segments (Fig. 1) was placed manually on SUV images of short-axis and vertical long-axis slices. The total SUV (T-SUV) was calculated as the sum of the values for all 13 segments in all 22 patients.

Semiquantitative visual analysis of the SPECT data was performed. Short-axis and vertical long-axis slices of the SPECT images were divided into 13 segments in the same manner as for PET. Segmental uptake of the tracer was graded by visual assessment using a 4-point scoring system (0 = normal; 1 = mild reduction; 2 = moderate reduction; and 3 = severe reduction in tracer uptake or absence of tracer uptake). The total defect score (TDS) was calculated as the sum of the scores for all 13 segments.

Abnormal myocardial ^{67}Ga uptake was considered present when abnormal intensity was clearly observed in anterior projections of the heart.

SPECT and scintigraphic images were interpreted independently by 2 experienced nuclear physicians who had no prior information about the clinical and histopathologic data. The examination was followed by discussion until a consensus was reached.

Statistical Analysis

Data are expressed as mean ± SD. Sensitivities of fasting ^{18}F-FDG PET, ^{99m}Tc-MIBI SPECT, and ^{67}Ga scanning for detecting myocardial lesions of sarcoidosis were compared using the Fisher exact test. The Student *t* test for unpaired data was used to examine differences between groups. Correlations between the 2 values were analyzed by simple linear regression analysis or the Spearman rank correlation test. Differences were considered significant when $P < 0.05$.

RESULTS

Blood Glucose

Fasting plasma blood glucose concentrations were 72–104 mg/dL in group A, 74–104 mg/dL in group B, and 75–103 mg/dL in healthy volunteers. No significant differences were apparent between groups with respect to the mean blood glucose level.
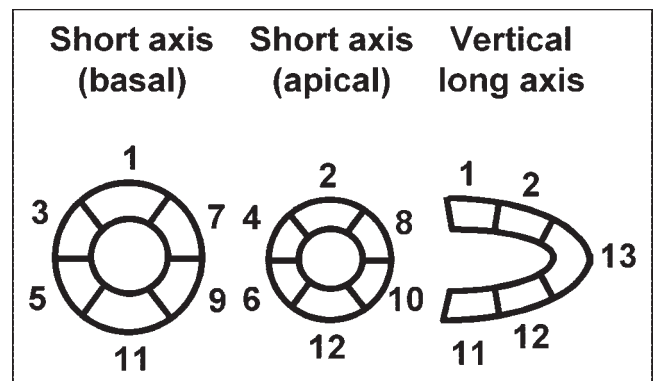
FIGURE 1. Short-axis and vertical long-axis slices of myocardial PET and SPECT images were divided into 13 segments.

TABLE 3
SUV of ^{18}F-FDG for Each of 13 Myocardial Segments in Healthy Volunteers

Parameter	Myocardial segment												
	1	2	3	4	5	6	7	8	9	10	11	12	13
Mean	1.94	1.92	1.89	1.85	1.87	1.87	1.98	1.95	1.94	1.93	1.93	1.92	1.86
SD	0.20	0.21	0.19	0.23	0.19	0.25	0.20	0.24	0.18	0.20	0.22	0.26	0.16
Mean + 2 SD	2.34	2.33	2.28	2.30	2.26	2.37	2.39	2.42	2.29	2.34	2.37	2.44	2.18

Normal Segmental SUV

In healthy volunteers, the mean + 2 SD of the SUV was calculated for each of the 13 myocardial segments to determine the normal upper level of the SUV (Table 3). A segmental SUV greater than this level was defined as abnormal in this study. No statistically significant differences were observed between the SUV for each segment among healthy volunteers.

Frequency of Abnormal Segments

A total of 143 myocardial segments were analyzed both in group A and in group B. The results of segmental analysis of myocardial nuclear imaging using ^{18}F-FDG PET and ^{99m}Tc-MIBI SPECT are summarized in Table 4.

In group A, abnormal uptake of ^{18}F-FDG was observed in all patients. Among the total 143 myocardial segments examined in group A patients, 73 segments exhibited an abnormal high SUV (range, 2.51–14.70; mean, 6.16). A segmental perfusion abnormality on ^{99m}Tc-MIBI SPECT occurred in 33 segments (mean DS = 2.1; range, 1–3) in 7 patients. The mean number of abnormal segments per patient (frequency of abnormal segments) was 6.6 ± 3.0 (range, 3–13) on ^{18}F-FDG PET, which was significantly higher than that on ^{99m}Tc-MIBI SPECT (3.0 ± 3.2; range, 0–10) ($P < 0.05$).

Histologic and Clinical Cardiac Sarcoidosis

The frequency of segments demonstrating abnormal ^{18}F-FDG uptake in patients with histologic cardiac sarcoidosis (patients 1–3) was 4.7 segments per patient (range, 4–6), which was lower than that in patients with clinical cardiac sarcoidosis (7.4; range, 3–13); however, this trend did not reach statistical significance (Fig. 2A). The frequency of segments with abnormal ^{99m}Tc-MIBI uptake in patients with histologic cardiac sarcoidosis was significantly higher than that in those with clinical cardiac sarcoidosis (Fig. 2B). The mean T-SUV was significantly lower in patients with histologic cardiac sarcoidosis as compared with that in those with clinical cardiac sarcoidosis (Fig. 2C). Conversely, the mean TDS was significantly higher in patients with histologic cardiac sarcoidosis as compared with that in those with clinical cardiac sarcoidosis (Fig. 2D).

Relationships Between Imaging Abnormality and Clinical Data

Table 4 summarizes the TDS on ^{99m}Tc-MIBI SPECT and the T-SUV on ^{18}F-FDG PET for each patient. Among group A patients, a statistically significant correlation was observed between the TDS and left ventricular ejection fraction (LVEF) ($r = -0.82$, $P < 0.01$) (Fig. 3A), whereas no significant correlation was found between the T-SUV and LVEF. Furthermore, the T-SUV and serum ACE level showed a good linear correlation ($y = 0.22x + 4.46$; $r = 0.83$; $P < 0.01$) (Fig. 3B), but the TDS was not correlated with serum ACE. No significant correlation was found between the TDS and T-SUV (data not shown).

Segmental Analysis

We also performed particular studies on the myocardial segments with abnormal nuclear imaging findings in order to clarify the clinical pathophysiologic relationships between inflammatory activity and myocardial damage in myocardial lesions of cardiac sarcoidosis. We classified myocardial segments into the following 4 types based on the findings of 2 nuclear imaging techniques: normal segment = normal ^{18}F-FDG uptake with normal ^{99m}Tc-MIBI perfusion ($n = 54$), matched abnormal segment = abnormal ^{18}F-FDG uptake with abnormal ^{99m}Tc-MIBI perfusion ($n = 17$), mismatched segment = abnormal ^{18}F-FDG uptake with normal ^{99m}Tc-MIBI perfusion ($n = 56$), and inverse mismatched segment = normal ^{18}F-FDG uptake with abnormal ^{99m}Tc-MIBI perfusion ($n = 16$). Further studies were performed on the 3 types of abnormal segments (matched abnormal, mismatched, and inverse mismatched segment) as described below.

SUV in Segments with Abnormal ^{18}F-FDG Uptake. SUV was significantly lower in matched abnormal segments (range, 2.51–8.30) than in mismatched segments (range, 3.18–14.70) (mean values, 4.77 ± 2.06 vs. 6.58 ± 3.00, $P < 0.01$). SUV was significantly correlated with DS in the segments with abnormal ^{18}F-FDG uptake ($r = -0.33$, $P < 0.01$) (Fig. 4A).

DS in Segments with Abnormal ^{99m}Tc-MIBI Perfusion. The mean DS of matched abnormal segments was significantly lower than that of inverse mismatched segments (1.82 ± 0.53 vs. 2.31 ± 0.48, $P < 0.01$). Significant correlations were found between the DS and SUV in segments with abnormal ^{99m}Tc-MIBI perfusion ($r = -0.48$, $P < 0.01$) (Fig. 4B).

Relationships Between SUV and DS in Abnormal Segments. In the 3 types of abnormal segments (matched abnormal, mismatched, and inverse mismatched), a statistically significant negative correlation was found between SUV and DS ($r = -0.63$, $P < 0.0001$) (Fig. 4C).

TABLE 4
Results of Myocardial Nuclear Imaging

Patient no.	67Ga*	Seg. 1		Seg. 2		Seg. 3		Seg. 4		Seg. 5		Seg. 6		Seg. 7		Seg. 8		Seg. 9		Seg. 10		Seg. 11		Seg. 12		Seg. 13		18F-FDG	99mTc-MIBI	T-SUV of 18F-FDG	TDS of 99mTc-MIBI
Group A																															
1	+	**3.51**	(0)	**3.54**	(0)	2.13	**(3)**	**3.18**	(0)	1.84	**(2)**	1.62	**(2)**	2.08	(0)	2.14	(0)	1.74	(0)	2.03	(0)	1.77	(0)	**2.51**	**(2)**	2.01	(0)	**4**	**4**	30.1	9
2	+	**3.82**	(0)	**4.12**	(0)	**3.08**	**(2)**	**4.03**	**(2)**	2.08	(0)	1.87	(0)	2.12	(0)	1.83	(0)	1.94	(0)	1.68	(0)	1.64	**(2)**	1.60	**(2)**	1.78	(0)	**4**	**4**	31.6	8
3	−	2.84	**(2)**	**3.81**	(0)	**2.51**	**(3)**	**2.82**	**(2)**	1.89	**(3)**	1.61	**(2)**	**2.64**	**(2)**	**3.54**	(0)	1.68	**(2)**	1.83	(0)	1.95	**(3)**	1.95	**(2)**	1.87	**(3)**	6	10	30.9	24
4	−	**14.13**	(0)	**6.20**	**(1)**	**8.70**	(0)	2.24	(0)	2.13	(0)	2.02	(0)	**14.70**	(0)	**9.41**	(0)	**6.60**	(0)	**4.48**	(0)	2.06	(0)	2.13	(0)	**5.98**	(0)	8	1	80.8	1
5	−	**5.23**	(0)	**4.82**	(0)	**4.47**	(0)	2.21	(0)	1.98	(0)	1.71	(0)	**4.98**	(0)	**4.16**	(0)	**3.88**	(0)	1.90	(0)	1.82	(0)	1.80	(0)	2.13	(0)	6	0	41.1	0
6	+	**6.88**	(0)	**7.31**	(0)	2.23	**(2)**	2.20	**(2)**	**4.72**	**(2)**	2.08	**(3)**	**10.94**	(0)	**11.12**	(0)	**7.79**	(0)	**9.32**	(0)	**9.20**	(0)	**7.60**	**(1)**	**6.11**	**(2)**	10	6	87.5	12
7	+	**4.31**	(0)	**4.97**	(0)	2.04	(0)	1.93	(0)	1.73	(0)	1.78	(0)	**3.25**	**(2)**	**3.82**	**(2)**	1.95	(0)	1.91	(0)	1.83	**(2)**	1.75	(0)	1.80	**(2)**	**4**	**4**	33.1	8
8	−	2.21	(0)	2.14	(0)	1.95	(0)	1.98	(0)	1.84	(0)	1.78	(0)	**5.44**	(0)	**4.88**	(0)	**5.13**	(0)	2.10	(0)	2.01	(0)	1.83	(0)	1.90	(0)	3	0	35.2	0
9	−	**5.74**	(0)	**5.12**	(0)	**4.18**	(0)	**4.24**	(0)	**3.64**	(0)	**3.56**	(0)	**5.01**	(0)	**4.76**	(0)	1.74	(0)	1.95	(0)	2.28	(0)	1.83	(0)	1.78	(0)	8	0	45.8	0
10	−	**13.81**	(0)	**9.94**	(0)	**6.71**	**(2)**	**8.34**	(0)	**6.15**	**(2)**	**8.56**	(0)	**12.02**	(0)	**9.78**	(0)	**9.91**	(0)	**9.53**	(0)	**7.78**	**(1)**	**8.30**	**(1)**	**6.90**	(0)	13	4	117.7	6
11	−	**9.54**	(0)	2.30	(0)	**6.51**	(0)	**4.91**	(0)	**6.02**	(0)	**3.71**	(0)	2.21	(0)	**4.41**	(0)	1.97	(0)	2.01	(0)	2.12	(0)	**4.25**	(0)	1.89	(0)	7	0	51.9	0
																												Sum 73	33		
Group B																															
12	−	2.10	(0)	1.98	(0)	1.88	(0)	1.71	(0)	1.76	(0)	1.81	(0)	2.14	(0)	2.01	(0)	1.98	(0)	1.89	(0)	1.74	(0)	1.80	(0)	1.89	(0)	0	0	24.7	0
13	−	1.56	(0)	1.61	(0)	1.41	(0)	1.53	(0)	1.43	(0)	1.45	(0)	1.69	(0)	1.79	(0)	1.88	(0)	1.61	(0)	1.79	(0)	1.78	(0)	2.01	(0)	0	0	21.5	0
14	−	1.78	(0)	1.83	(0)	1.88	(0)	1.71	(0)	1.63	(0)	1.72	(0)	1.97	(0)	1.94	(0)	1.93	(0)	2.01	(0)	2.11	(0)	2.01	(0)	1.79	(0)	0	0	24.3	0
15	−	1.91	(0)	1.82	(0)	1.79	(0)	1.85	(0)	1.90	(0)	1.85	(0)	2.15	(0)	2.08	(0)	2.17	(0)	1.83	(0)	1.65	(0)	1.72	(0)	1.89	(0)	0	0	24.6	0
16	−	2.18	(0)	2.08	(0)	1.92	(0)	1.95	(0)	2.08	(0)	1.89	(0)	1.82	(0)	1.79	(0)	1.70	(0)	1.71	(0)	1.94	(0)	1.91	(0)	1.99	(0)	0	0	25.0	0
17	−	1.98	(0)	2.17	(0)	1.91	(0)	2.05	(0)	1.86	(0)	1.99	(0)	1.99	(0)	2.09	(0)	1.80	(0)	1.82	(0)	1.75	(0)	1.72	(0)	1.73	(0)	0	0	24.9	0
18	−	2.04	(0)	1.89	(0)	2.15	(0)	2.08	(0)	1.87	(0)	1.71	(0)	1.65	(0)	1.70	(0)	1.88	(0)	1.99	(0)	2.11	(0)	1.86	(0)	1.98	(0)	0	0	24.9	0
19	−	1.97	(0)	2.13	(0)	2.07	(0)	1.78	(0)	2.05	(0)	1.90	(0)	2.27	(0)	2.29	(0)	2.10	(0)	2.15	(0)	2.19	(0)	2.29	(0)	1.62	(0)	0	0	26.8	0
20	−	1.72	(0)	1.60	(0)	1.85	(0)	1.77	(0)	1.88	(0)	2.07	(0)	1.91	(0)	1.88	(0)	1.67	(0)	1.97	(0)	1.99	(0)	1.96	(0)	1.97	(0)	0	0	24.2	0
21	−	2.03	(0)	1.99	(0)	2.21	(0)	2.08	(0)	2.06	(0)	1.99	(0)	1.79	(0)	2.11	(0)	2.18	(0)	2.20	(0)	2.00	(0)	1.99	(0)	1.81	(0)	0	0	26.4	0
22	−	**3.11**	(0)	**2.81**	(0)	**3.13**	(0)	**2.77**	(0)	1.91	(0)	2.12	(0)	**3.30**	(0)	**3.13**	(0)	**3.10**	(0)	**3.07**	(0)	1.81	(0)	1.95	(0)	2.10	(0)	8	0	34.3	0
																												Sum 8	0		

*+ represents myocardial uptake of 67Ga; − represents no myocardial uptake of 67Ga.
†Data for each segment (Seg.) are presented as SUV; score in parentheses represents DS. Boldface values represent abnormal data.
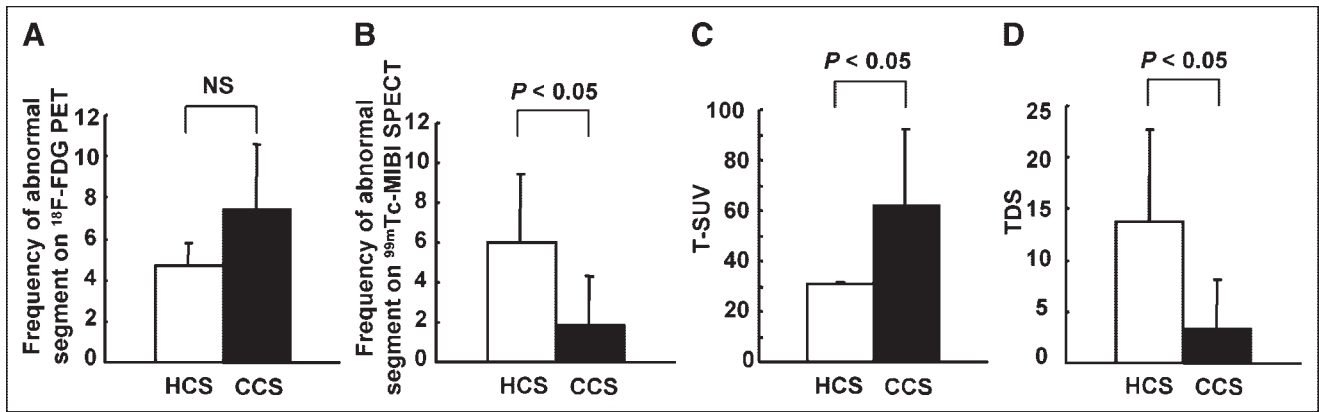
FIGURE 2. Comparison of nuclear measurements between histologically diagnosed cardiac sarcoidosis (HCS) and clinically diagnosed cardiac sarcoidosis (CCS). Frequency of abnormal segments on ^{99m}Tc-MIBI SPECT and TDS in HCS (white bar) was significantly higher than that in CCS (black bar) (B and D). In contrast, frequency of abnormal segments on fasting ^{18}F-FDG PET and T-SUV in HCS were lower than those in CCS, although significant difference could be observed only for T-SUV (A and C). NS = not significant.

Localization and Distribution of Abnormal Segments. Localization of the 3 types of abnormal segment is summarized in Figure 5. Mismatched segments were frequently observed in the basal and mid anteroseptal-lateral wall of the left ventricle (LV), whereas inverse mismatched segments had a tendency to localize in the septal and inferior wall of the LV and matched abnormal segments showed no tendency to localize. Abnormal segments showed discontinuous distribution in only 2 patients (patients 7 and 11), being distributed continuously in the other 9 patients.

Sensitivity and Specificity

Using the guidelines for diagnosing cardiac sarcoidosis provided by the Japanese Ministry of Health and Welfare as a gold standard, we calculated the sensitivity, specificity, and accuracy of ^{18}F-FDG PET, ^{99m}Tc-MIBI SPECT, and ^{67}Ga scintigraphy for the detection of cardiac sarcoidosis (Table 5). Abnormal ^{18}F-FDG uptake was observed in all group A patients, resulting in a sensitivity of 100%, which

was significantly higher than that of ^{99m}Tc-MIBI SPECT or ^{67}Ga scintigraphy (63.6% and 36.4%, respectively). With regard to specificity, no significant differences were found between imaging modalities. The accuracy of ^{18}F-FDG PET, ^{99m}Tc-MIBI SPECT, and ^{67}Ga scintigraphy was 95.5% (21/22), 81.8% (18/22), and 68.2% (15/22), respectively. Although the accuracy of ^{18}F-FDG PET was higher than that of the other nuclear imaging modalities, a significant difference was observed only with respect to ^{67}Ga scintigraphy.

DISCUSSION

The main results of this study can be summarized as follows: (a) Fasting ^{18}F-FDG PET can be performed in patients with sarcoidosis for the detection of myocardial abnormalities and results in more frequent detection of abnormalities than either ^{99m}Tc-MIBI SPECT or ^{67}Ga scintigraphy. (b) Fasting ^{18}F-FDG PET can provide useful information with regard to the extent and activity of inflammation in cardiac sarcoidosis in the particular condition. (c) Semiquantitative analysis using fasting ^{18}F-FDG PET in combination with ^{99m}Tc-MIBI SPECT can simultaneously evaluate regional inflammatory activity and perfusion abnormalities. In this regard, our results demonstrated fewer perfusion abnormalities in those myocardial segments exhibiting high inflammatory activity.

Several studies have previously shown the diagnostic value of ^{18}F-FDG PET in myocardial involvement of sarcoidosis (*7,8*). However, to our knowledge, this is the first study concerning the diagnostic accuracy of fasting ^{18}F-FDG PET in detecting inflammatory lesions of cardiac sarcoidosis from a pathophysiologic standpoint, based on correlative analysis between uptake patterns shown by combined nuclear imaging studies and clinical and histologic findings.
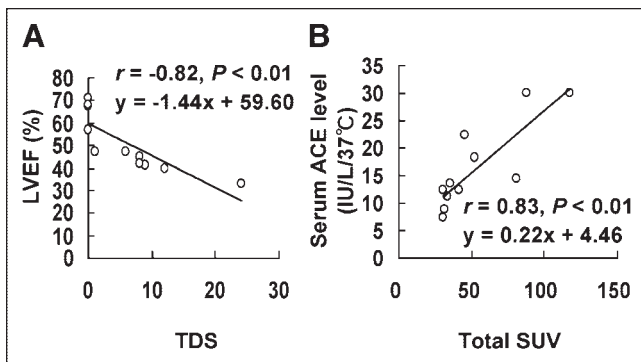
FIGURE 3. Relationship between nuclear measurements (T-SUV and TDS) and clinical data (LVEF and serum ACE level) in patients with cardiac sarcoidosis (group A). Statistically significant correlations were observed between TDS and LVEF (A) and between T-SUV and serum ACE level (B).
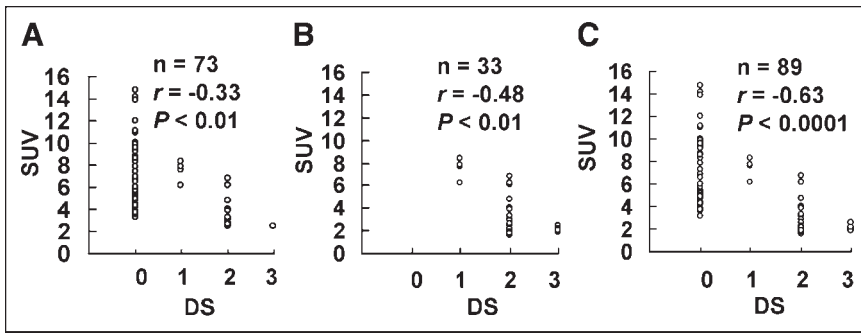
FIGURE 4. Correlation between SUV and DS in segments with abnormal ^{18}F-FDG uptake (A), those with abnormal ^{99m}Tc-MIBI perfusion (B), and those with abnormal ^{18}F-FDG uptake or ^{99m}Tc-MIBI defect (C). Significant negative correlations were observed in all types of abnormal segment.

Diagnostic Accuracy

Evidence of increased glucose metabolism in inflamed tissue has been demonstrated by various experimental studies (11,12). Newsholme and Newsholme demonstrated that inflammatory cells in an activated state produce 7- to 8-fold higher levels of ATP when compared with those under baseline conditions (13). Mauel also showed significantly increased glucose oxidation through the hexose monophosphate shunt pathway when murine macrophages were exposed to dilutions of the bacterial extract OM-86BV (14). Macrophages are known to have high rates of protein secretion and membrane recycling. Indeed, rapidly dividing cells, such as activated inflammatory cells, have high glycolytic activity to satisfy their large energy demands, a fact that is supported by evidence of increased metabolic activity noted during immunologic responses (13). Histologic studies of biopsy specimens suggest that macrophages, which contribute to granuloma formation, are activated (15). This may explain in part why granulomatous lesions demonstrate high uptake of ^{18}F-FDG.

FDG is a glucose analog that traces the transmembranous transport and hexokinase-mediated phosphorylation of glucose. FDG-6-phosphate is then effectively trapped within the myocyte, because the sarcolemma is relatively impermeable to this intermediate, which is a poor substrate for further metabolism by either glycolytic or glycogen-synthetic pathways, and because dephosphorylation of FDG-6-phosphate is thought to be quite slow. The regional distribution of myocardial activity, assessed 40–60 min after intravenous administration of FDG, is believed to be related to overall (anaerobic and aerobic) regional glycolytic flux (16).

In normal myocardium, metabolism is primarily oxidative and utilizes various admixtures of substrates (free fatty acids, glucose, and lactate). The proportional contribution of each substrate to overall oxidative metabolism is dependent on multiple factors, including arterial substrate content, the hormonal milieu, and the temporal relationship to a myocardial ischemic insult (17,18). Under fasting conditions, plasma insulin levels fall, resulting in reduced transport of glucose into myocytes and an increase in the availability of free fatty acids secondary to increased lipolysis in peripheral adipose tissue. Under these conditions, free fatty acids become the preferred energy substrate for oxidative metabolism, whereas the contribution of glucose to total energy production via oxidative metabolism is decreased. Elevation of plasma fatty acids leads to inhibition of absolute glucose utilization by the heart (19) and results in subtraction of background myocardial ^{18}F-FDG uptake, causing more distinct visualization of ^{18}F-FDG accumulation in inflammatory lesions. Therefore, small absolute differences in glucose utilization between inflamed and normal myocardium may appear relatively large under these conditions. It is reasonable to consider fasting ^{18}F-FDG PET as a suitable method to detect the metabolic sequelae of inflammatory lesions of cardiac sarcoidosis because it accentuates the difference between inflamed tissue (increased
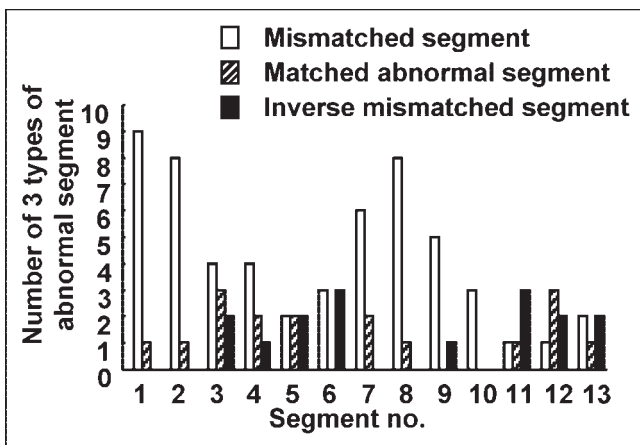
FIGURE 5. Localization of 3 types of abnormal segment.

TABLE 5
Diagnostic Performance of Fasting ^{18}F-FDG PET, ^{99m}Tc-MIBI SPECT, and ^{67}Ga Scintigraphy

Parameter	Percentage (no. of patients)		
	^{18}F-FDG PET	^{99m}Tc-MIBI SPECT	^{67}Ga scintigraphy
Sensitivity	100 (11/11)	63.6* (7/11)	36.4† (4/11)
Specificity	90.9 (10/11)	100 (11/11)	100 (11/11)
Accuracy	95.5 (21/22)	81.8 (18/22)	68.2* (15/22)

*$P < 0.05$ vs. ^{18}F-FDG PET.
†$P < 0.01$ vs. ^{18}F-FDG PET.

accumulation of ^{18}F-FDG) and normal tissue (less uptake). For these reasons, fasting ^{18}F-FDG PET was shown to be preferable in this study, demonstrating higher performance in detecting myocardial involvement of sarcoidosis as compared with the other nuclear diagnostic imaging modalities. In addition to high spatial resolution, the particular metabolic setting described here was considered to play an important role in the superior diagnostic performance of fasting ^{18}F-FDG PET in detecting cardiac sarcoidosis.

Pathophysiologic Considerations

It is generally accepted that interstitial pneumonitis with mononuclear cell infiltration of macrophages and lymphocytes represents a very early lesion, possibly the initial lesion, in pulmonary sarcoidosis, predating the appearance of characteristic epithelioid granulomas. Several clinical and experimental investigations support this view of histologic development in sarcoidosis, confirming that epithelioid granuloma formation is preceded by a diffuse mononuclear cell infiltration in all sites where granulomas are found (20–23). It was recently reported that monocyte chemoattractant protein-1, an important mediator of monocyte infiltration in the monocyte/macrophage-mediated inflammatory process (24–26), was markedly increased in the early stage of pulmonary sarcoidosis and was significantly correlated with serum ACE levels (27). In contrast, as the granuloma matures, the numbers of epithelioid cells increase and the numbers of monocytes, macrophages, and lymphocytes decline (20,28). In patients with progressive lesions containing numerous granulomas, alveolitis is minimal or absent (20). Additionally, a well-developed characteristic epithelioid granuloma is encircled by antiinflammatory T-lymphocytes, which fulfill the function of suppressing granulomatous formation (29). This evidence strongly indicates that the inflammatory reaction is more prominent in the early stage of sarcoidosis compared with the advanced stage of the disease in which characteristic granulomas develop. This results in a higher population of activated macrophages in the early disease. It has been clearly demonstrated that ^{18}F-FDG accumulates in macrophages and reactive lymphocytes of inflammatory tissue (30). Activated monocytes/macrophages and T-lymphocytes in inflammatory tissue use glucose as an energy source for chemotaxis and phagocytosis (31) and can increase both oxygen consumption and glucose metabolism in response to immune reactions (32). However, clinical investigations using PET that take into account the pathophysiology of cardiac sarcoidosis have not yet been reported.

In the segmental analysis of this study, normal segments represented myocardium with normal perfusion and no inflammatory lesion, mismatched segments represented normal perfusion and active inflammatory lesion (early stage of disease), matched abnormal segments represented abnormal perfusion and active inflammatory lesion (advanced stage of disease), and inverse mismatched segments represented abnormal perfusion and no inflammatory lesion (end-stage of disease). Myocardial segments with a DS of 3 on ^{99m}Tc-MIBI imaging are considered to represent fibrotic degeneration and 6 segments showed a DS of 3 in the present study. Interestingly, 5 of these 6 segments showed a normal SUV of ^{18}F-FDG and the SUV was almost normal in the remaining segment, indicating that, in end-stage myocardium, active inflammatory lesions are no longer present. This premise is supported by the striking finding that the SUV of affected myocardial segments showed a negative correlation with DS.

On the other hand, comparative study between histlogic cardiac sarcoidosis and clinical cardiac sarcoidosis demonstrated that the mean T-SUV of a patient with histologic cardiac sarcoidosis was significantly lower than that of clinical cardiac sarcoidosis. In contrast, the mean TDS of histologic cardiac sarcoidosis was significantly higher than that of clinical cardiac sarcoidosis. This evidence might indicate that clinical cardiac sarcoidosis predominantly represents an early stage of the disease with mononuclear cell infiltration containing abundant macrophages preceding formation of epithelioid granuloma and that histologic cardiac sarcoidosis mainly represents a mature stage of the disease with numerous granulomas. This stage would result in a high prevalence of positive histologic findings on endomyocardial biopsy examination. However, positive findings on endomyocardial biopsy were also found in patients with localized lesions (patients 1 and 2). Because the number of patients with positive findings on endomyocardial biopsy in this study might be too small to draw conclusions from statistical analysis, studies should be performed in a larger population to confirm our results.

It is now apparent that sarcoid lesions can originate at different times (33,34) in the same organ. Therefore, the myocardium of patients with cardiac sarcoidosis would be expected to contain various stages of inflammatory lesions with varying severity. This speculation is supported by our finding that almost group A patients demonstrated various types of abnormal segments at the same time (Table 4). Our results (Table 4) also demonstrate that different stages in the natural history of cardiac sarcoidosis could be recognized in each patient according to the characteristic distribution of the 3 types of abnormal segment and the combined pattern of T-SUV and TDS. The patients in group A can be longitudinally classified from a pathophysiologic standpoint as follows: those in the early stage of disease (patients 5, 8, 9, and 11; high T-SUV with a TDS of 0), the progressive inflammatory stage (patient 4; very high T-SUV with low TDS), the peak active stage (patient 10; extremely high T-SUV with moderately high TDS), the progressive myocardial impairment stage (patient 6; very high T-SUV with high TDS), and the fibrosis-dominant, low-activity stage (patients 1–3 and 7; low T-SUV with high TDS). Patients 1 and 2 might represent those with localized lesions and patient 22 might have the early stage of the disease. Two representative cases (patient 9 [early stage] and patient 1

[fibrosis-dominant low-activity stage]) are shown in Figures 6 and 7.

In summary, these results indicate that myocardial segments with high inflammatory activity (high SUV level) show less myocardial involvement (lower DS), indicating the early stage of sarcoid lesions. Conversely, our results indicate that myocardial segments with severe myocardial involvement (high DS) considered to be progressive myocardial lesions show less inflammatory activity (low SUV level) and that end-stage myocardial fibrosis (DS of 3) no longer exhibits active inflammatory lesions (normal or near-normal SUV).

Significance of Fasting ^{18}F-FDG PET in Cardiac Sarcoidosis

Conventional SPECT with ^{201}Tl or ^{99m}Tc-MIBI is used to detect myocardial involvement in cardiac sarcoidosis. However, the abnormalities demonstrated in these SPECT images do not represent early lesions but, instead, signify impaired myocardium in the progressive stage. In contrast, abnormal ^{18}F-FDG uptake on fasting ^{18}F-FDG PET is seen in active inflammatory lesions at the early stage of cardiac sarcoidosis. Therefore, fasting ^{18}F-FDG PET is a particularly appropriate imaging modality for detecting the early stage of myocardial lesions, in which high inflammatory activity precedes severe myocardial involvement, rather than the advanced stage of the disease. Clinically, this method might therefore represent a promising technique for diagnosis of the early stage of cardiac sarcoidosis and thus be valuable in providing adequate treatment. This could help prevent myocardial involvement and possible irreversible end-stage fibrosis.

On the other hand, the significance of rest scintigraphic perfusion defects remains in question. Granuloma with scar fibrosis or microcirculatory dysfunction has been considered as a cause for perfusion defects on myocardial SPECT in cardiac sarcoidosis (6,35,36). A previous study found that patients with idiopathic dilated cardiomyopathy exhibited
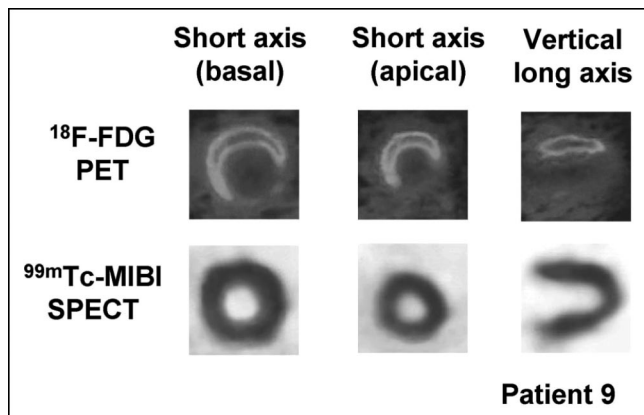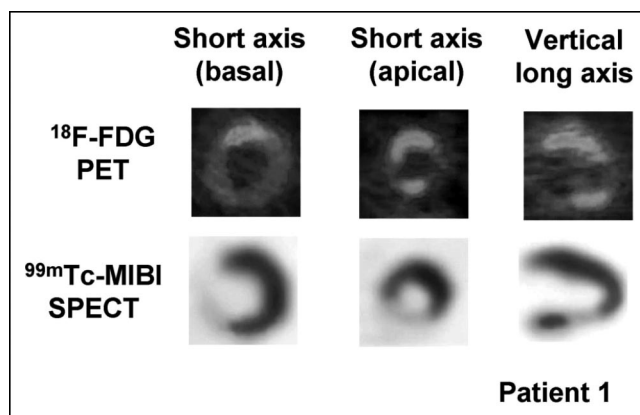
FIGURE 7. Fasting ^{18}F-FDG PET images (top) and ^{99m}Tc-MIBI SPECT images (bottom) in patient 1. ^{18}F-FDG PET revealed slightly increased uptake of ^{18}F-FDG in segments 1, 2, 4, and 12. ^{99m}Tc-MIBI SPECT clearly revealed moderate reduction of ^{99m}Tc-MIBI uptake in segments 5, 6, and 12 and severe reduction of ^{99m}Tc-MIBI uptake in segment 3.

heterogeneous myocardial glucose uptake (37), and a more recent study reported that increased uptake of ^{18}F-FDG was found in myocardial segments with anaerobic metabolism in the patients with idiopathic dilated cardiomyopathy (38). This indicates that increased uptake of ^{18}F-FDG positively correlates with ischemic involvement in the patients with idiopathic dilated cardiomyopathy. In cardiac sarcoidois, if vasoconstrictive ischemia of the microvasculature is induced by the inflammatory process and accounts for myocardial ^{99m}Tc-MIBI perfusion defects, myocardial perfusion abnormality would show a positive correlation with ^{18}F-FDG uptake. However, in the present study, myocardial perfusion abnormality showed an impressive negative correlation with myocardial ^{18}F-FDG uptake in patients with cardiac sarcoidosis who showed normal coronary angiographic findings. Although ^{99m}Tc-MIBI defects might be partially dependent on microvascular vasoconstriction, our data indicated that scar fibrosis was the main mechanism of the ^{99m}Tc-MIBI perfusion defect.

Limitations

The use of high-dose corticosteroids has been encouraged in the hope that it may alter the course of the cardiac sarcoidosis if started early (39,40). In this study, the response of fasting ^{18}F-FDG PET to steroid treatment in patients with cardiac sarcoidosis was not investigated. A recent study found that cardiac ^{13}N-NH$_3$/^{18}F-FDG PET under fasting conditions was useful both in identification of cardiac involvement of sarcoidosis and in following inflammatory response to therapy (7). However, to our knowledge, there are no pathophysiologic studies with segmental analysis that investigate the usefulness of fasting ^{18}F-FDG PET for the evaluation of steroid therapy in cardiac sarcoidosis. Serial and longitudinal pathophysiologic investigation of fasting ^{18}F-FDG PET using segmental analysis of the natural and treated course of sarcoidosis is necessary to further

FIGURE 6. Fasting ^{18}F-FDG PET images (top) and ^{99m}Tc-MIBI SPECT images (bottom) in patient 9. ^{18}F-FDG PET revealed markedly increased uptake of ^{18}F-FDG in segments 1–8, whereas ^{99m}Tc-MIBI SPECT revealed no abnormal findings.

delineate the clinical usefulness of this method in the management of this disease.

CONCLUSION

In this study, we investigated the usefulness of fasting ^{18}F-FDG PET for the detection of myocardial involvement in patients with cardiac sarcoidosis detected using orthodox diagnostic criteria for cardiac sarcoidosis. Fasting ^{18}F-FDG PET detected abnormalities more frequently than either ^{99m}Tc-MIBI SPECT or ^{67}Ga scintigraphy in patients with cardiac sarcoidosis. Segmental nuclear analysis using combined imaging with fasting ^{18}F-FDG PET and ^{99m}Tc-MIBI SPECT suggested that fasting ^{18}F-FDG PET could detect the early stage of cardiac sarcoidosis that is associated with less perfusion abnormalities and greater active inflammation. These results indicate that fasting ^{18}F-FDG PET is an appropriate imaging modality suitable for the diagnosis of cardiac sarcoidosis in the clinical setting, particularly in the early stage of myocardial involvement before advanced myocardial impairment.

REFERENCES

1. Silverman KJ, Hutchins GM, Bulkley BH. Cardiac sarcoid: a clinicopathologic study of 84 unselected patients with systemic sarcoidosis. *Circulation.* 1978;58:1204–1211.
2. Perry A, Vuitch F. Cause of death in patients with sarcoidosis: a morphologic study of 38 autopsies with clinicopathologic correlations. *Arch Pathol Lab Med.* 1995;119:167–172.
3. Iwai K, Tachibana T, Takemura T, Matsui Y, Kitaichi M, Kawabata Y. Pathological studies on sarcoidosis autopsy. I. Epidemiological features of 320 cases in Japan. *Acta Pathol Jpn.* 1993;43:372–376.
4. Sharma OP, Maheshwari A, Thaker K. Myocardial sarcoidosis. *Chest.* 1993;103:253–258.
5. Okayama K, Kurata C, Tawarahara K, Wakabayashi Y, Chida K, Sato A. Diagnostic and prognostic value of myocardial scintigraphy with thallium-201 and gallium-67 in cardiac sarcoidosis. *Chest.* 1995;107:330–334.
6. Le Guludec D, Menad F, Faraggi M, Weinmann P, Battesti JP, Valeyre D. Myocardial sarcoidosis: clinical value of technetium-99m sestamibi tomoscintigraphy. *Chest.* 1994;106:1675–1682.
7. Yamagishi H, Shirai N, Takagi M, et al. Identification of cardiac sarcoidosis with ^{13}N-NH3/^{18}F-FDG PET. *J Nucl Med.* 2003;44:1030–1036.
8. Takeda N, Yokoyama I, Hiroi Y, et al. Positron emission tomography predicted recovery of complete A-V nodal dysfunction in a patient with cardiac sarcoidosis. *Circulation.* 2002;105:1144–1145.
9. Hiraga H, Hiroe M, Iwai K, et al. *Guideline for Diagnosis of Cardiac Sarcoidosis: Study Report on Diffuse Pulmonary Disease* [in Japanese]. Tokyo, Japan: Japanese Ministry of Health and Welfare; 1993:23–24.
10. Inoue T, Shibasaki T, Oriuchi N, et al. ^{18}F-α-Methyl tyrosine PET studies in patients with brain tumors. *J Nucl Med.* 1999;40:399–405.
11. Amaral JF, Shearer JD, Mastrofrancesco B, Gann DS, Caldwell MD. Can lactate be used as a fuel by wounded tissue? *Surgery.* 1986;100:252–261.
12. Daley JM, Shearer JD, Mastrofrancesco B, Caldwell MD. Glucose metabolism in injured tissue: a longitudinal study. *Surgery.* 1990;107:187–192.
13. Newsholme P, Newsholme EA. Rates of utilization of glucose, glutamine and oleate and formation of end-products by mouse peritoneal macrophages in culture. *Biochem J.* 1989;261:211–218.
14. Mauel J. Macrophage activation by OM-85BV. *Respiration.* 1992;59(suppl 3):14–18.
15. Dannenberg AM Jr. Macrophages in inflammation and infection. *N Engl J Med.* 1974;293:489–493.
16. Ratib O, Phelps ME, Huang SC, Henze E, Selin CE, Schelbert HR. Positron tomography with deoxyglucose for estimating local myocardial glucose metabolism. *J Nucl Med.* 1982;23:577–586.
17. Merhige ME, Ekas R, Mossberg K, Taegtmeyer H, Gould KL. Catecholamine stimulation, substrate competition, and myocardial glucose uptake in conscious dogs assessed with positron emission tomography. *Circ Res.* 1987;61(suppl II):124–129.
18. Myears DW, Sobel BE, Bergmann SR. Substrate use in ischemic and reperfused canine myocardium: quantitative considerations. *Am J Physiol.* 1987;253:H107–H114.
19. Wisneski JA, Gertz EW, Neese RA, Gruenke LD, Morris DL, Craig JC. Metabolic fate of extracted glucose in normal human myocardium. *J Clin Invest.* 1985;76:1819–1827.
20. Rosen Y, Athanassiades TJ, Moon S, Lyons HA. Nongranulomatous interstitial pneumonitis in sarcoidosis: relationship to development of epithelioid granulomas. *Chest.* 1978;74:122–125.
21. Teilum G. Morphogenesis and development of sarcoid lesions: similarities to the group of collagenosis. *Acta Med Scand.* 1964;425(suppl):14–18.
22. Spector WG, Heesom N. The production of granulomata by antigen-antibody complexes. *J Pathol.* 1969;98:31–39.
23. Unanue ER, Benacerraf B. Immunologic events in experimental hypersensitivity granulomas. *Am J Pathol.* 1973;71:349–360.
24. Jones ML, Warren JS. Monocyte chemoattractant protein 1 in a rat model of pulmonary granulomatosis. *Lab Invest.* 1992;66:498–503.
25. Warren JS, Jones ML, Flory CM. Analysis of monocyte chemoattractant protein 1-mediated lung injury using rat lung organ cultures. *Am J Pathol.* 1993;143:894–906.
26. Antoniades HN, Neville-Golden J, Galanopoulos T, Kradin RL, Valente AJ, Graves DT. Expression of monocyte chemoattractant protein 1 mRNA in human idiopathic pulmonary fibrosis. *Proc Natl Acad Sci USA.* 1992;89:5371–5375.
27. Iyonaga K, Suga M, Ichiyasu H, Yamamoto T, Hiraga Y, Ando M. Measurement of serum monocyte chemoattractant protein-1 and its clinical application for estimating the activity of granuloma formation in sarcoidosis. *Sarcoidosis Vasc Diffuse Lung Dis.* 1998;15:165–172.
28. Soler P, Basset F. Morphology and distribution of cells of a sarcoid granuloma: ultrastructural study of serial sections. *Ann NY Acad Sci.* 1976;278:147–160.
29. Kita S, Tsuda T, Sugisaki K, Miyazaki E, Matsumoto T. Characterization of distribution of T lymphocyte subsets and activated T lymphocytes infiltrating into sarcoid lesions. *Intern Med.* 1995;34:847–855.
30. Yamada S, Kubota K, Kubota R, Ido T, Tamahashi N. High accumulation of fluorine-18-fluorodeoxyglucose in turpentine-induced inflammatory tissue. *J Nucl Med.* 1995;36:1301–1306.
31. Weisdorf DJ, Craddock PR, Jacob HS. Glycogenolysis versus glucose transport in human granulocytes: differential activation in phagocytosis and chemotaxis. *Blood.* 1982;60:888–893.
32. Fantone JC, Ward PA. Role of oxygen-derived free radicals and metabolites in leukocyte-dependent inflammatory reactions. *Am J Pathol.* 1982;107:395–418.
33. Mitchell DN, Scadding JG. Sarcoidosis. *Am Rev Respir Dis.* 1974;110:774–802.
34. Mitchell DN, Scadding JG, Heard BE, Hinson KFW. Sarcoidosis: histopathological definition and clinical diagnosis. *J Clin Pathol.* 1977;30:395–408.
35. Bulkley BH, Rouleau JR, Whitaker JQ, Strauss HW, Pitt B. The use of 201-thallium for myocardial perfusion imaging in sarcoid heart disease. *Chest.* 1977;72:27–32.
36. Tellier P, Paycha F, Antony I, et al. Reversibility by dipyridamole of thallium-201 myocardial scan defects in patients with sarcoidosis. *Am J Med.* 1988;85:189–193.
37. Yokoyama I, Momomura S, Ohtake T, et al. Role of positron emission tomography using fluorine-18 fluoro-2-deoxyglucose in predicting improvement in left ventricular function in patients with idiopathic dilated cardiomyopathy. *Eur J Nucl Med.* 1998;25:736–743.
38. van den Heuvel AF, van Veldhuisen DJ, van der Wall EE, et al. Regional myocardial blood flow reserve impairment and metabolic changes suggesting myocardial ischemia in patients with idiopathic dilated cardiomyopathy. *J Am Coll Cardiol.* 2000;35:19–28.
39. Lorell B, Alderman EL, Mason JW. Cardiac sarcoidosis: diagnosis with endomyocardial biopsy and treatment with corticosteroid. *Am J Cardiol.* 1978;42:143–146.
40. Ishikawa T, Kondoh H, Nakagawa S, Koiwaya Y, Tanaka K. Steroid therapy in cardiac sarcoidosis: increased left ventricular contractility concomitant with electrocardiographic improvement after prednisolone. *Chest.* 1984;85:445–447.